Journal: Energy & Fuels

Special Issue: In Honor of Michael J. Antal

DOI: 10.1021/acs.energyfuels.6b01024

Thermoanalytical characterization and catalytic conversion of de-oiled micro algae and jatropha seed cake

Zoltán Sebestyén[1*], Eszter Barta-Rajnai[1], Zsuzsanna Czégény[1], Thallada Bhaskar[2], Bhavya B. Krishna[2], Zoltán May[1], János Bozi[1], Zsolt Barta[3], Rawel Singh[2], Emma Jakab[1]

*sebestyen.zoltan@ttk.mta.hu

[1]*Institute of Materials and Environmental Chemistry, Research Centre for Natural Sciences, Hungarian Academy of Sciences, Magyar tudósok körútja 2, H-1117 Budapest, Hungary*

[2] *Bio-Fuel Division (BFD), CSIR-Indian Institute of Petroleum (IIP), Mohkampur, Dehradun-248005, Uttarakhand, India*

[3]*Department of Applied Biotechnology and Food Science, Budapest University of Technology and Economics, H-1111 Budapest, Szent Gellért tér 4, Hungary*

Abstract: The thermal decomposition of the by-products of the biodiesel process was studied by thermoanalytical methods. De-oiled algae cake and jatropha seed de-oiled cake were pyrolyzed and the catalytic effects of silica supported iron catalysts (Fe/FSM-16 and Fe/SBA-15) and magnetite (Fe_3O_4) were tested. The evolution profiles of the decomposition products as well as the thermal stability of the samples were determined by thermogravimetry/mass spectrometry (TG/MS). The formation of the volatile products was monitored by pyrolysis-gas chromatography/mass spectrometry (Py-GC/MS). The composition and the amounts of the

gaseous products changed significantly in the presence of the silica supported iron catalysts: the yield of hydrogen and carbon monoxide considerably increased above the decomposition temperature of 400 °C. Both silica supported iron catalysts had important effects on the yield of the products originating from carbohydrates and lignins. The formation of anhydrosugars and phenolic compounds was hindered, while the evolution of aromatic and aliphatic hydrocarbons was enhanced. Fe/FSM-16 proved to be more efficient than Fe/SBA-15 and Fe_3O_4 catalysts. The thermal decomposition of the protein content of the samples resulted in the formation of 2,5-diketopiperazines and smaller molecules (e.g., ammonia). The silica supported iron catalysts had a special effect: their presence promoted the reaction of fatty acid esters and ammonia resulting in the formation of alkyl nitriles during the thermal decomposition.

Keywords: Algae, jatropha seed, pyrolysis-gas chromatography/mass spectrometry, thermogravimetry/mass spectrometry, magnetite, Fe/FSM-16, Fe/SBA-15

1 INTRODUCTION

The applied mineral oil and natural gas can be partially substituted by renewable energy carriers hereby decreasing the consumption of fossil fuels. Biodiesel becomes more and more popular as a substitute for fossil transport fuels. Therefore, it is important to find novel renewable raw materials for the biodiesel production.

Algae are aquatic plants, which synthesize organic compounds from simple substances present in the surrounding water using light energy. Microalgae can be utilized in several ways, producing four types of renewable energy carriers: biodiesel,[1,2] bioethanol, hydrogen[3] and biogas;[4] moreover it is used in the nutrition, and cosmetic industry.[5] The algal oil can be extracted and

converted into biodiesel using different catalysts in a fixed bed reactor as reported by Krohn et al.[6] Biodiesel can be produced by various methods as demonstrated in the literature.[2,7,8] The bioenergy content of algae can be utilized by transformation into bioethanol, as well.[3] Green algae are able to generate hydrogen from water during the photosynthesis.[9] It means that hydrogen fuel could be produced essentially from water and sunlight if the appropriate technology were developed.[9-11] At the end of their life cycle microalgae should be utilized for other purposes. Microalgae have lower lignin and hemicellulose content[12] comparing to the terrestrial plants, but they contain protein, which has to be taken into consideration during the biomass utilization process.

Jatropha is a genus of flowering plants belonging to the family of *Euphorbiaceae*. This bushy tree is indigenous to America and India. Jatropha is one of the best candidates for the biodiesel production in India because about 40% of the seed mass is oil.[13] This opportunity is widely studied mainly in the habitat of this plant species, e.g., in India,[14] Tanzania[15] and Malaysia.[16] Jatropha seeds contain carcinogen phorbol molecules[17-19] and highly poisonous toxalbumins, [17] hence the by-products of the oil production are not suitable for animal nutrition.

The thermal conversion of the solid residues of the oil extraction process from jatropha seeds and microalgae may be a promising way to generate advanced biofuels from biomass by-products. The decomposition processes can be more efficient by applying suitable catalysts because the composition of the pyrolysis products can be more advantageous or the pyrolysis temperature can be decreased resulting in energy saving.

The pyrolysis oil originating from plant biomass has numerous oxygen-containing organic compounds, which reduce the quality of the product. Various types of catalysts have been tested in order to lower the oxygen content of the oil, including zeolites and metal oxides.[20] HZSM-5

zeolite was found as a promising catalyst to convert microalgae into aromatic hydrocarbons and ammonia by catalytic pyrolysis.[20]

SBA-15 mesoporous silica nanoparticles were prepared for the first time by Zhao and co-workers in 1998.[21,22] SBA-15 has a highly ordered hexagonal structure with the pore size of 5-30 nm prepared in the presence of triblock poly(ethylene oxide)-poly(propylene oxide)-poly(ethylene oxide) copolymer (PEO-PPO-PEO) as a template.[21,22] SBA-15 has a large specific surface area and high thermal stability hence it can be applied as an acidic catalyst support. Iron substituted SBA-15 catalyst is mostly applied to ozonation of different chemicals[23] and reformation of ethanol to a hydrogen rich gas mixture.[24]

A highly ordered mesoporous catalyst support (FSM-16) can be synthesized from kanemite mineral.[25,26] The hexagonal FSM-16 support has a large specific surface area with the pore size of 2-10 nm.[27] The iron substituted FSM-16 was successfully applied, e.g., in waste plastics pyrolysis,[28] Friedel-Crafts alkylation reaction[29] and in photocatalytic reaction for hydrogen production.[30] Silica, alumina and silica-alumina supported iron catalysts were used during recycling of waste lubricant oil. The catalysts promoted the cracking of the higher hydrocarbons into fuel oil.[31] Magnetite is commonly used as a catalyst in several reaction types, e.g., organic reactions,[32] ammonia synthesis and degradation of organic contaminants.[33]

In this study we report the catalytic effects of mesoporous silica (SBA-15 and FSM-16) supported iron catalysts with the goal of upgrading the thermal decomposition products of de-oiled algae and jatropha seed cakes. Magnetite (Fe_3O_4) catalyst was used for comparison with the silica supported iron catalysts because Fe_3O_4 iron phase had been formed in the supported catalysts after calcination. The efficiency of the catalysts was tested by thermogravimetry/mass spectrometry (TG/MS) and pyrolysis-gas chromatography/mass spectrometry (Py-GC/MS) techniques.

2 EXPERIMENTAL SECTION

2.1. Preparation of de-oiled algal cake (DAC). Algae were collected from natural water bodies in Telangana, India and they were cultivated in a wastewater pond. The algal biomass sample consists of different alga species: *Scenedesmus dimorphus, Scenedesmus quadricauda, Scenedesmus obliquus, Chlorella vulgaris, Chlorella minutissima* and *Chlorella protothecoide*. The dried wastewater algal biomass was subjected to sonication in order to disrupt the algal cell wall. The oil extraction was performed using n-hexane in a Soxhlet extraction apparatus. After several cycles of run the concentrated oil solution was transferred into a flask and the solvent was evaporated using a rotary evaporator. The de-oiled algae powder was washed by hot water at 60 °C for 2 hours in order to eliminate the main part of the water soluble organic and inorganic compounds of the sample.

2.2 Preparation of jatropha seed de-oiled cake (JSDC). Jatropha seeds originate from a local jatropha plantation in Uttarakhand, India. Jatropha seeds were mechanically crushed and pressed in order to separate the liquid fraction from the solid residue. The solid phase fraction was dried and milled to <100 μm particle size.

2.3 Catalysts. Mesoporous silica SBA-15 and FSM-16 supported iron catalysts were used to upgrade the thermal decomposition products of DAC and JSDC. The silica supported catalysts were prepared by wet impregnation method with iron loading of 5 wt%. As a catalyst, magnetite (Fe_3O_4) powder was tested as well. The catalysts were mixed with the biomass samples in the ratio of 1:1 in order to ensure the contact between the catalyst and the evolving gas phase decomposition products.

2.4. Thermogravimetry/mass-spectrometry (TG/MS). The TG/MS system consists of a modified Perkin-Elmer TGS-2 thermobalance and a Hiden HAL quadrupole mass spectrometer.

About 4 mg de-oiled algae and jatropha seed samples were measured in argon atmosphere at a flow rate of 140 ml min^{-1}. Approximately 6-7 mg samples were applied in case of the algae and jatropha seed mixed with the catalysts in the ratio of 1:1. The samples were heated at a rate of 20 °C min^{-1} from 25 to 900 °C in a platinum sample pan. The evolved products were introduced through a glass lined metal capillary heated at 300 °C into the ion source of the mass spectrometer which was operated at 70 eV electron energy.

2.5. Pyrolysis-gas chromatography/mass spectrometry (Py-GC/MS). Approximately 3 mg de-oiled algae cake and 1.5 mg jatropha seed de-oiled powders were pyrolyzed at 550 °C for 20 s in helium atmosphere using a Pyroprobe 2000 pyrolyzer interfaced to an Agilent 6890A/5973 GC/MS. The sample sizes were doubled in case of the biomass and catalyst mixtures. We applied relatively large sample sizes in order to ensure a better contact between the decomposition products of biomass samples and the catalysts. The interface and the GC injector were heated to 280 °C. The pyrolysis products were separated on a DB-1701 capillary column (30 m × 0.25 mm, 0.25 μm film thickness). The GC oven was programmed to hold at 40 °C for 4 min then increase the temperature at a rate of 6 °C min^{-1} to 280 °C (hold for 7 min). The mass range of *m/z* 14-500 was scanned at a rate of 3 scans s^{-1} by the mass spectrometer in electron impact mode at 70 eV electron energy. Two or three replicates were carried out with each sample.

2.6. Inductively coupled plasma-optical emission spectrometry (ICP-OES). About 2 g samples were ashed at 550 °C in a furnace according to an EU standard method CEN/TS 14775:2004. Ashes were fused at 920 °C with a fusion blend ($Li_2B_4O_7$:$LiBO_2$, 2:1) and digested by 25 mL 33% nitric acid. The inorganic ion contents of the samples were determined by a Spectro Genesis ICP-OES equipment (Spectro Analytical Instruments) with axial plasma observation using the

scanning range of 175-770 nm. The amounts of the ashes have been determined using the CEN/TS 14775 EU standard method.

2.7. Protein and carbohydrate contents. The crude protein contents of the DAC and JSDC powders were measured by the Dumas method.[34] The samples were combusted in an oxygen-rich environment at about 1000 °C and the evolving nitrogen gas was measured with a thermal conductivity detector (Leco protein analyzer FP528). The carbohydrate contents were determined according to the method of Sluiter et al.[35] applying slight modifications: the de-oiled algae and jatropha powders were treated in a two-step acidic hydrolysis with 72% H_2SO_4 for 2 hours at room temperature, and then with 4% H_2SO_4 for 1 hour at 121 °C. The suspensions obtained were filtered and washed with distilled water through G4 glass filter crucibles. The sugar concentrations of the filtered supernatants were analyzed with high performance liquid chromatography (HPLC) using an Agilent 1260 instrument (Agilent Technologies, USA). An Aminex HPX-87H column (Bio-Rad, Hercules, CA, USA) at 65 °C and a refractive index detector were applied. An eluent of 5 mM H_2SO_4 was used at a flow rate of 0.5 ml min^{-1}. The solid residues obtained after washing were dried at 105 °C until constant weight. The dried residue consisted of acid-insoluble organics (e.g., lignin) and acid-insoluble ash. The total ash and acid-insoluble ash contents were measured after ashing the samples at 550 °C (4 hours) to avoid the decomposition of calcium carbonate.

3 RESULTS AND DISCUSSION

3.1 Chemical composition of the biomass residues. Table 1 shows the composition of the samples including the organic and inorganic contents. The cellulose and hemicellulose contents of the biomass samples were determined using HPLC analysis after acidic hydrolysis. The de-oiled algal cake powder contains 4.1% cellulose, while the cellulose content of the de-oiled

jatropha seed is much higher (15.7%). About 7.3% of DAC and 24.2% of JSDC is insoluble in 72% H_2SO_4 solution. These data characterize the acid insoluble lignin content of the samples. According to the Dumas method, DAC and JSDC samples have relatively high protein concentrations, 21 and 29%, respectively. The DAC sample has 52.8% ash, while the ash content of JSDC is only 10.5%. Considering the high ash content of DAC it can be established that protein represents about 43% of the organic materials of DAC, while the carbohydrate and lignin contents of DAC are significantly lower than that of JSDC. This difference can be observed generally in the composition of aquatic and terrestrial plants. Furthermore, DAC contains significantly higher amounts of extractables and/or acid soluble lignin than JSDC, which can be explained probably by the higher residual oil content of the de-oiled algae sample.

Table 1. Composition of the De-oiled Samples Studied.

Components	De-oiled algal cake (DAC)	Jatropha seed de-oiled cake (JSDC)
Organic components, m-%, db[a]		
Cellulose	4.1	15.7
Hemicellulose	2.3	11.4
Acid insoluble lignin	7.3	24.2
Protein	20.5	28.8
Other (e.g., extractables, acid soluble lignin)	13.0	9.4
Ash at 550°C (m-%), db[a]	52.8	10.5
Inorganic components, ppm[b]		
K^+	6005	15971
Na^+	3373	219
Mg^{2+}	16475	9180
Ca^{2+}	112187	10009
P	6557	11598
S	2070	2192

[a]Dry basis
[b]Calculated for the dry, total biomass sample

It is well-known that the thermal decomposition mechanisms as well as the product distribution of the biomass samples are considerably affected by the alkali ion concentration.[36] Therefore the composition of the ash was determined by ICP-OES measurements and the concentrations of the inorganic ions and elements were recalculated for the basis of dry biomass samples. As Table 1 shows, the potassium ion concentration of DAC is about 6000 ppm, while JSDC has almost 3 times higher K^+ content. The Na^{2+} content of JSDC is negligible. DAC has relatively high sodium, magnesium and calcium ion contents comparing to the jatropha seed cake. It is in agreement with literature data on the composition of various algae[37] and terrestrial plants.[38] The high concentration of these ions can be explained by the fact that algae are aquatic organisms and the sample was grown in a wastewater. The DAC sample contains high amount of Ca^{2+} mostly in the form of carbonate (as discussed below). The higher inorganic concentration of DAC comparing to JSDC explains the higher ash content, as well.

3.2 TG/MS results. Figure 1 presents the thermogravimetric (TG) and derivative thermogravimetric (DTG) curves of DAC and JSDC as well as the same samples mixed with Fe/FSM-16, Fe/SBA-15 and Fe_3O_4 catalysts. The oil content of the algae and jatropha seeds was removed during the processing, which explains the lower organic content and the high ash content (Table 1.) and therefore the relatively high carbonaceous residue contents (char) of the samples (Figure 1a and 1c).

TG (Figure 1a and 1c) and DTG (Figure 1b and 1d) curves show that the thermal decomposition of the de-oiled algae powders occurs in three main stages, while the jatropha seed de-oiled cake decomposes in two main steps. The first peak on the DTG curves between 50 and 180 °C can be attributed to the evaporation of the adsorbed water. The thermal decomposition of the organic compounds (e.g., carbohydrates, proteins, and residual oil) starts at 200 °C and ends at about 560 °C. The main DTG peak has one or two shoulders indicating the different thermal stability of the

various organic components. The DAC sample generates a third intensive DTG peak at around 700 °C, which can be attributed to the decomposition of calcium carbonate (Figure 1b). Studying the effect of the applied iron catalysts on the decomposition rate of organic compounds in DAC and JSDC samples (Figure 1b and 1d), it can be seen that the decomposition rate is significantly lower up to 400 °C in the presence of both applied silica supported catalyst. Using Fe_3O_4 this effect is less characteristic in case of DAC and the decomposition rate of the organic materials of JSDC is not affected by Fe_3O_4.

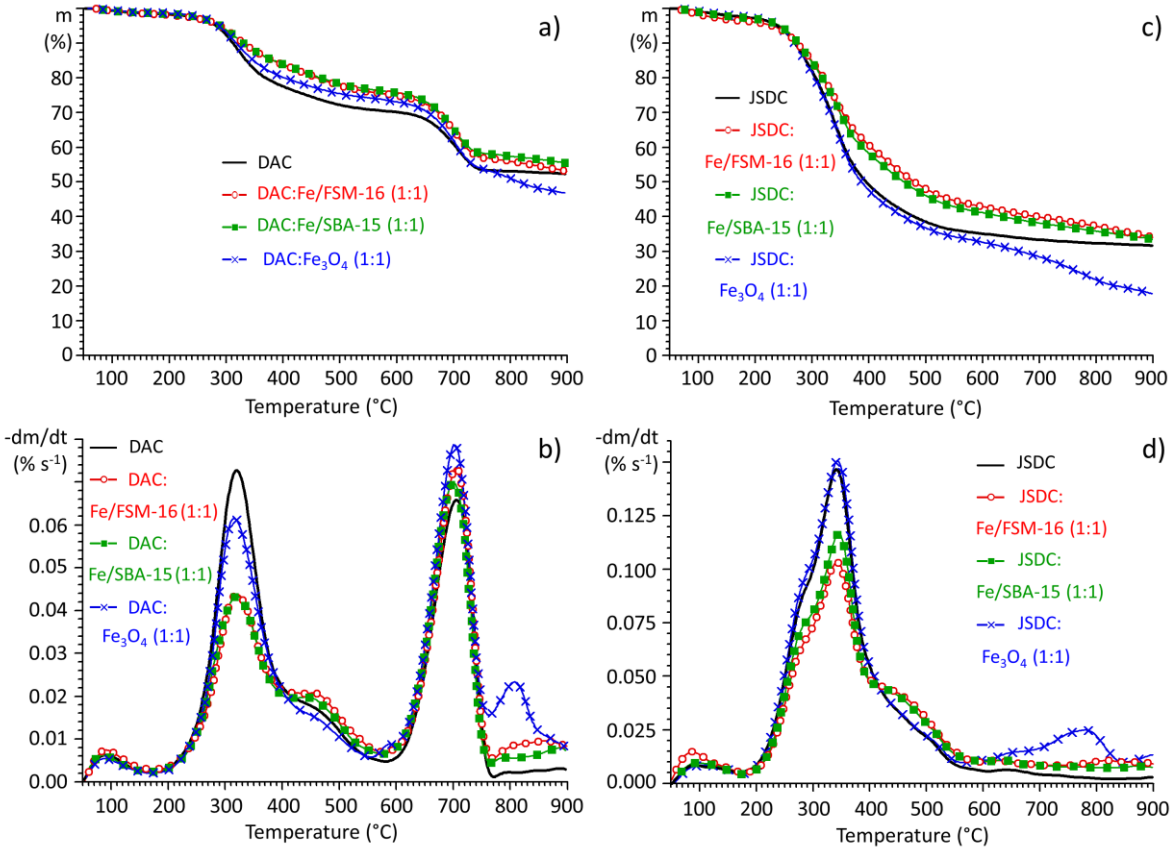

Figure 1. (a, c) TG and (b, d) DTG curves of the de-oiled algae cake (DAC) and the jatropha seed de-oiled cake (JSDC) with and without the catalysts.

Figure 2 presents the evolution profiles of the main gaseous products of DAC with and without catalysts. The effect of the catalysts on the evolution profile of the same ions of JSDC is very

similar; therefore these results have been placed into the Supporting Information as Figure S1. Between 400 and 560 °C a characteristic shoulder can be seen on the DTG curve, which is slightly more intensive using the silica supported iron catalysts. The ion intensity curve at *m/z* 29 shows two maxima in each case. The first peak on the evolution profile of *m/z* 29 ion (at around 310 °C) can be attributed to the CHO^+ fragment of the aldehyde compounds. The second peak of *m/z* 29 ion (at about 450 °C) overlaps with the characteristic shoulder of the DTG curve.

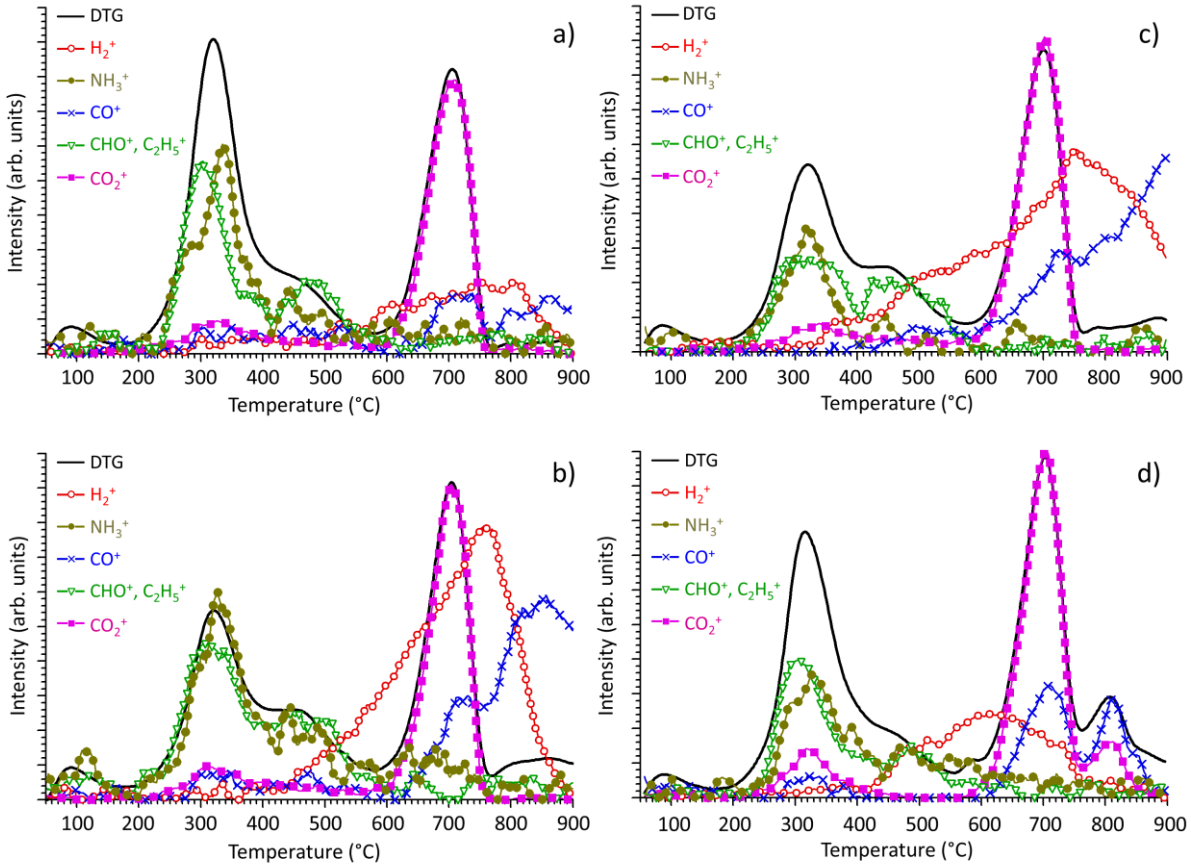

Figure 2. Evolution profiles of the main gaseous decomposition products (*m/z* 2, hydrogen; *m/z* 17, ammonia; *m/z* 28, carbon monoxide; *m/z* 29, formyl and ethyl groups; *m/z* 44, carbon dioxide) derived from the de-oiled algae cake (DAC) (a) without catalysts, in the presence of (b) Fe/FSM-16, (c) Fe/SBA-15, and (d) Fe_3O_4 catalysts.

The weight loss in this temperature range can be attributed most probably to the decomposition of the remaining oil fraction of algae. The *m/z* 29 ion curve at around 450 °C (Figure 2) mostly represents ethyl group, which is a mass spectrometric fragment ion of the hydrocarbons. The presence of alkane and 1-alkene decomposition products in the pyrolyzate (see later) also supports this assumption. The evolution profiles of the mass spectrometric curve at *m/z* 17 represent the formation of ammonia during the TG/MS measurements. It should be noted that water also has a fragment ion at *m/z* 17; however, its intensity was subtracted from the total intensity of *m/z* 17. The main source of the evolving ammonia is the protein content of the samples (Table 1), which is about 20% in case of DAC. The catalysts hinder the ammonia production to some extent.

The final decomposition step of the DAC sample takes place between 600 and 800 °C. The inorganic carbonate content (mostly calcium carbonate) decomposes into metal oxide and carbon dioxide as the evolution curve of CO_2 (*m/z* 44) implies in Figure 2. Further charring reactions of the solid residue also take place indicated by the release of hydrogen and carbon-monoxide. When using Fe_3O_4 catalyst, there is another carbon dioxide peak at about 820 °C, which coincides with a high carbon monoxide peak (Figure 2d). This can be explained by the oxidation of the carbonaceous residue with Fe_3O_4 leading to the formation of CO and CO_2. This reaction can also be seen on the DTG curve of JSDC (Figure 1d). As a result of the char oxidation, the total weight loss of DAC and JSDC is the highest in the presence of magnetite. This reaction is much less significant when Fe/FSM-16 and Fe/SBA-15 were applied, which indicates that the iron bonded to the silica support material is not capable to oxidize the char at about 800 °C. The evolution of hydrogen and carbon monoxide from DAC sample is substantially more intensive using Fe/FSM-16 or Fe/SBA-15 catalysts, as shown in Figure 2b and 2c, while they are slightly increased in the presence of magnetite (Figure 2d). Similar catalytic effect was observed

in case of de-oiled jatropha seed sample. This observation can be related to the fact that the main devolatilization step between 200 and 400 °C is significantly hindered applying the silica supported iron catalysts. Apparently more hydrogen and oxygen remained in these samples, which are released in the form of H_2 and CO above 600 °C during the charring process.

3.3 Pyrolysis results. Pyrolysis-gas chromatography/mass spectrometry (Py-GC/MS) measurements have been performed to reveal the effect of iron catalysts on the pyrolysis product distribution of DAC and JSDC samples. On the basis of the TG curves (Figure 1), 550 °C pyrolysis temperature was selected representing the temperature of the complete decomposition of the organic materials. Above 550 °C only the decomposition of inorganic carbonates and charring reactions occur (between 600 and 900 °C).

Figure 3 and Figure 4 illustrate the pyrograms of DAC and JSDC (a) and the samples mixed with Fe/FSM-16 (b), Fe/SBA-15 (c) and magnetite (d) catalysts. Since the pyrolysis experiments were performed with small sample sizes, the catalysts were mixed with the samples in the ratio of 1:1 in order to make sure the contact between the decomposition products and the catalysts. The identification as well as the relative peak areas (%) of the pyrolysis products are listed in Table 2. In order to understand the changes in the chemical composition of the pyrolysis oil, the main decomposition products were organized into groups and the relative peak areas of these compounds were summed. These results are presented in Table 3 and in the pie charts found in the Supporting Information (Figure S2). The quantitative determination of the gaseous products is quite uncertain by Py-GC/MS due to the poor resolution, so the GC peaks eluting between 2.2 and 2.5 min retention times were omitted from the relative peak area % calculation. The identification of the molecules is based on their NIST mass spectral library and literature data.[39-42]

The unresolved peaks at lower retention times (**G** in Figure 3 and 4) represent the evolution of gaseous and vapor products of low molecular weight, e.g., carbon dioxide, water and methane, which may be formed by the scission of various functional groups of several components.

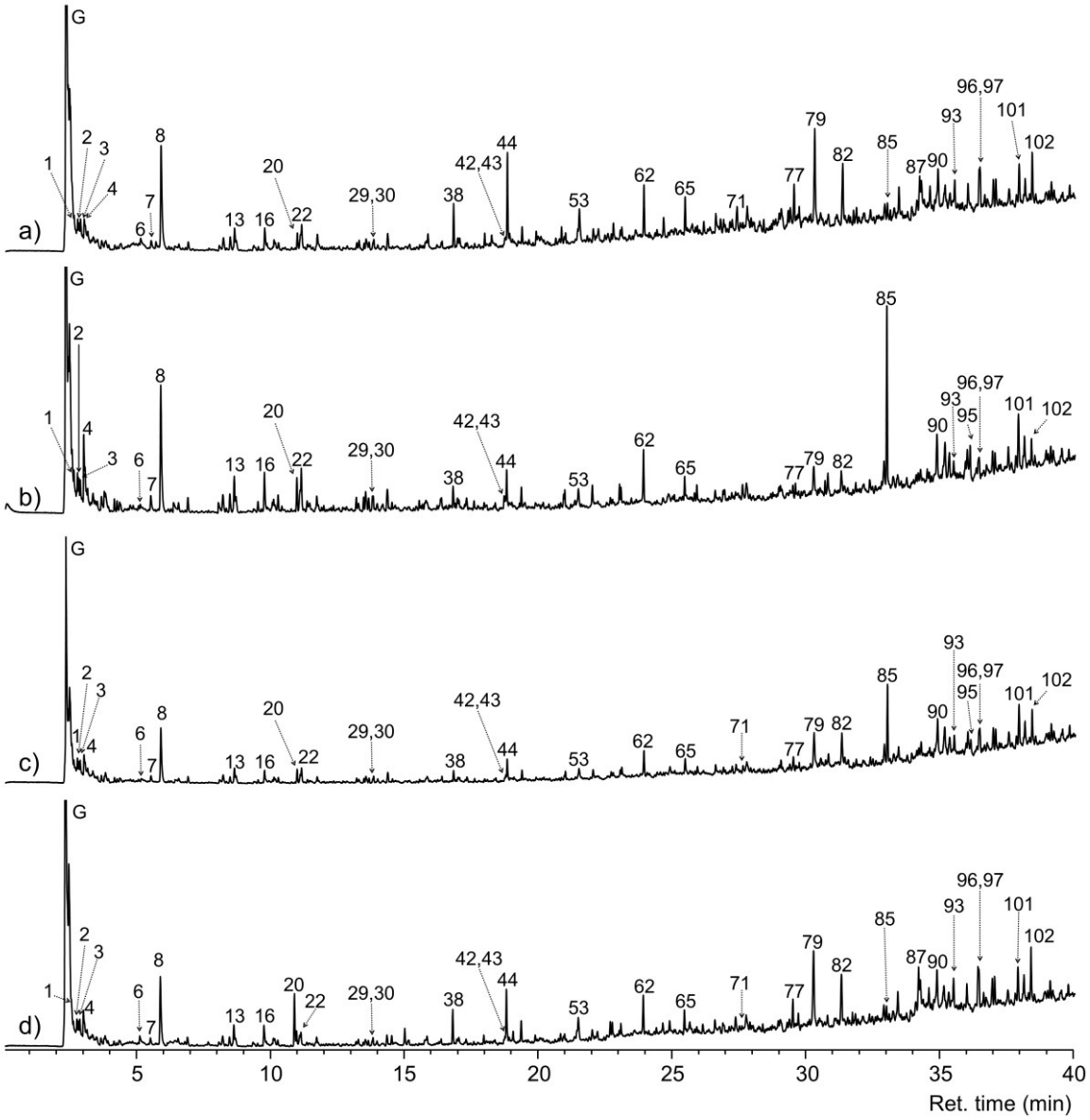

Figure 3. Pyrograms of (a) DAC, (b) DAC + Fe/FSM-16, (c) DAC + Fe/SBA-15 and (d) DAC + magnetite catalysts at 550 °C. Peak identities are given in Table 2.

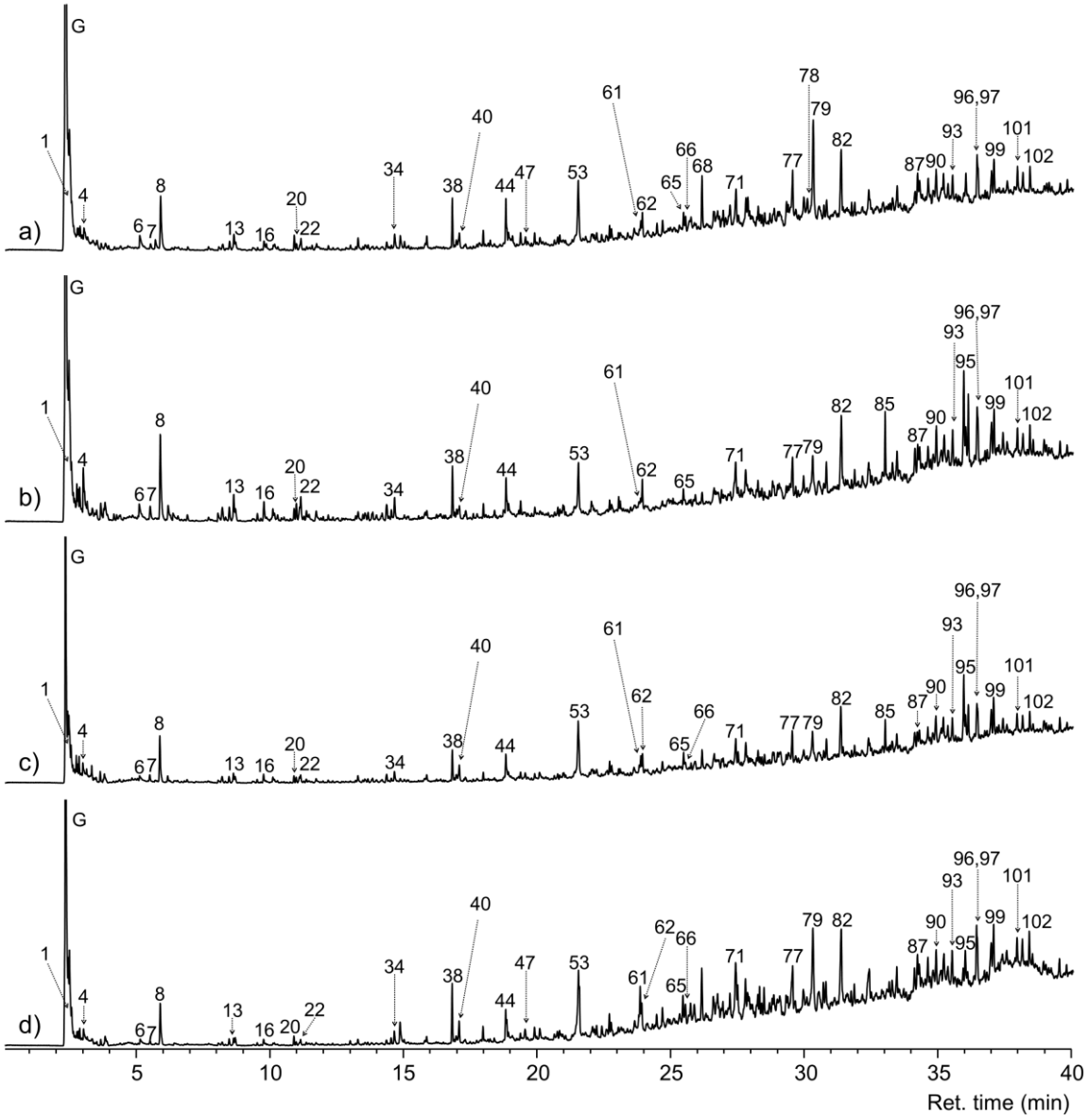

Figure 4. Pyrograms of (a) JSDC, (b) JSDC + Fe/FSM-16, (c) JSDC + Fe/SBA-15, and (d) JSDC + magnetite catalysts at 550°C. Peak identities are given in Table 2.

Table 2. The Main Decomposition Products Released in the Py-GC/MS Experiment at 550 °C of DAC and JSDC Samples with and without Catalysts. Peak Numbers refer to the Peaks in Figs. 3 and 4.

No.	RT (min)	Compounds	Most abundant ions, molecular ion (*m/z*)	Possible origin[a]	Area %[b] DAC	Area %[b] DAC Fe/FSM16	Area %[b] DAC Fe/SBA15	Area %[b] DAC Fe_3O_4	Area %[b] JSDC	Area %[b] JSDC Fe/FSM16	Area %[b] JSDC Fe/SBA15	Area %[b] JSDC Fe_3O_4
1	2.57	1-Pentene	42, 55, 70	E	2.52	3.22	2.74	2.48	2.74	1.73	2.17	1.51
2	2.83	Acetone	43, 58	CH	0.59	0.76	0.64	0.63	0.46	0.70	0.64	0.24
3	2.90	Hexane + 1-Hexene	41, 56, 86, 84	E	0.85	0.73	0.81	0.93	0.55	0.86	0.89	0.27
4	3.01	Acetonitrile	41, 40, 39	CH, P	1.38	2.66	1.21	1.46	0.94	2.07	0.63	0.65
5	3.81	Benzene	78, 52, 50	L, P					0.45	1.18	0.62	0.49
6	5.12	Acetic acid	43, 45, 60	H, L	1.13	0.26	0.71	0.72	1.41	1.10	1.90	0.55
7	5.51	Octane + 1-Octene	41, 55, 114, 112	E	0.57	1.05	0.61	0.43	0.45	0.93	0.61	0.23
8	5.90	Toluene	91, 92	L, P	6.90	8.13	5.23	5.44	3.57	5.46	3.24	2.24
9	6.90	3-Methylbutanenitrile	43, 41, 68, (83)	P	0.54	0.83	0.52	0.58				
10	8.06	2-Methylpyridine	93, 66, 78	P	0.38	0.74	0.36	0.24	0.25	0.57	0.18	0.16
11	8.21	Nonane + 1-Nonene	56, 41, 128, 126	E	0.89	1.22	0.86	0.81	0.42	0.94	0.73	0.19
12	8.46	Ethylbenzene	91, 106, 65	L, P	0.86	0.99	0.54	0.63	0.51	0.73	0.44	0.31
13	8.64	Pyrrole	67, 39, 41	P	1.29	1.79	1.21	1.39	0.91	1.38	0.81	0.36
14	8.69	p-Xylene	91, 106, 105	L, P	0.65	0.94	0.67	0.49	0.50	0.71	0.46	0.41
15	9.52	o,m-Xylene	91, 106, 105	-L, P	0.17	0.55	0.22	0.17	0.14	0.37	0.22	0.12
16	9.77	Styrene	104, 103, 78	L, P	1.26	2.15	0.90	1.37	0.58	1.11	0.58	0.25
17	10.11	2-Cyclopentene-1-one	82, 39, 54	CH	0.45	0.51	0.36	0.33	0.19	0.56	0.76	0.07
18	10.16	Furfural	96, 95, 39	CH	0.38	0.27	0.23	0.36	0.32	0.35	0.37	0.08
19	10.28	4-Methylpentanenitrile	55, 43, 41, (97)	P	0.42	0.80	0.40	0.29				
20	10.98	3-Methyl-1H-pyrrole	80, 81, 53	P	0.78	1.49	0.98	0.90	0.35	0.74	0.31	0.17
21	11.09	Decane + 1-Decene	70, 57, 142, 140	E	0.85	1.00	0.65	0.65		0.63	0.52	0.11
22	11.14	2-Methyl-1H-pyrrole	80, 81, 53	P	1.22	2.26	1.11	0.77	0.58	1.18	0.55	0.25
23	11.72	2-Methyl-2-cyclopenten-1-one	67, 53, 96	CH	0.86	0.83	0.50	0.57	0.30	0.68	0.55	0.15
24	13.19	2,3-Dimethyl-1H-pyrrole	94, 95, 80	P	0.42	0.63	0.40	0.22				
25	13.28	1,2-Cyclopentanedione	98, 55, 69	CH	0.69	0.53	0.38	0.43	0.74	0.46	0.60	0.35
26	13.46	2,3-Dimethyl-1H-pyrrole	94, 95, 80	P	0.29	0.60	0.30	0.19				
27	13.53	2,4-Dimethyl-1H-pyrrole	94, 95, 80	P	0.85	1.32	0.75	0.49				
28	13.65	2-Propenyl-benzene	117, 118, 115	L, P	0.45	0.72	0.37	0.29				
29	13.79	Undecane	57, 71, 134	E	0.29	0.61	0.43	0.17				
30	13.82	1-Undecene	55, 70, 132	E	0.51	0.58	0.51	0.42				
31	13.97	5-Methyl-2-furancarboxaldehyde	110, 109, 53	CH	0.34	0.50	0.47	0.24				
32	14.34	3-Methyl-2-cyclopenten-1-one	96, 67, 53	CH	1.07	1.46	0.99	0.74	0.54	0.95	0.74	0.26
33	14.52	Benzonitrile	103, 76, 50	P		0.36	0.24	0.52	0.19	0.46	0.19	0.30
34	14.64	Aniline	93, 66, 65	P					1.17	1.34	0.83	0.71
35	15.84	2-Hydroxy-3-methyl-2-cyclopenten-1-one	112, 55, 69	CH	0.83		0.89	0.65	0.62	0.42	0.60	0.34
36	16.34	Dodecane	57, 71, 170	E	0.17	0.44		0.10				
37	16.37	1-Dodecene	41, 55, 168	E	0.26	0.49	0.34	0.27				
38	16.80	Phenol	94, 66, 67	L, P	1.82	1.08	0.86	1.90	2.20	2.22	1.24	2.35
39	17.04	1H-Pyrrole-2,5-dione	97, 54, 69	P	0.52	0.46	0.33	0.50				
40	17.06	Guaiacol	109, 124, 81	L					1.17	0.59	1.52	1.16
41	17.95	2-Methylphenol	108, 107, 79	L	0.71	0.36	0.31	0.53	0.77	0.66	0.43	0.65
42	18.70	Tridecane	57, 43, 71, 184	E	0.34	0.57	0.23	0.23				
43	18.74	1-Tridecene	55, 69, 97, 182	E	0.47	0.49	0.41	0.44				
44	18.80	4-Methylphenol	107, 108, 77	L	3.60	1.93	1.82	3.00	1.89	1.58	1.42	1.19
45	18.83	3-Methylphenol	107, 108, 77	L					0.55	0.59	0.87	0.94
46	19.35	Benzylnitrile	117, 90, 116	P	0.92	0.92	0.82	1.15	0.73	0.72	0.57	0.31
47	19.52	Anhydrosugar	44, 57	CH					0.57			0.63
48	19.53	3-Methylguaiacol	138, 123	L					0.46		0.58	0.45
49	19.87	2,4-Dimethylphenol	122, 107, 121	L	0.76		0.37	0.50	0.67	0.52	0.34	0.57
50	20.81	4-Ethylphenol	107, 122, 77	L	0.90	0.40	0.27	0.47	0.49	0.31	0.16	0.68
51	20.93	Tetradecane	57, 43, 194	E	0.41	0.47	0.34	0.29				

52	20.97	1-Tetradecene	55, 69, 196	E	0.41	0.76	0.60	0.41					
53	21.48	2,5-Pyrrolidinedione	28, 99, 56	P	2.44	1.31	1.68	1.96	3.21	1.25	3.53	3.39
54	22.00	Benzene-propanenitrile	91, 131, 65	P	0.13	1.65	1.17	0.89				
55	22.20	1,4:3,6-dianhydro-α-D-glucopyranose	69, 57, 98, 144	C	0.72			0.65	0.63		0.34	0.65
56	22.67	1H-Pyrrole-2-carbonitrile	92, 65, 41	P		0.39	0.51	0.92				
57	22.67	4-Vinylguaiacol	137, 152	L					0.67	0.65	0.73	0.97
58	22.75	4-Vinylphenol	120, 91, 65	L	1.09	0.28	0.41	0.81	0.82	0.38	0.51	0.67
59	23.02	Pentadecane	57, 71, 212	E	0.49	0.87	0.51	0.35		0.69	0.34	
60	23.07	1-Pentadecene	55, 69, 210	E	0.59	0.75	0.74	0.65		0.58	0.36	
61	23.84	Syringol	154, 139, 111	L					0.94	0.45	1.22	2.11
62	23.90	Indole	117, 90, 89	P	2.30	2.60	2.11	2.20	1.44	1.63	1.12	1.35
63	24.44	Eugenol	164, 149, 103	L					0.83			0.63
64	24.64	Propiram	98, 42, 56, (275)	P	1.26			0.61	1.22	0.44	0.75	0.98
65	25.43	3-Methyl-1H-indole	130, 129, 77	P	1.86	1.08	1.71	1.58	1.20	0.72	1.43	1.35
66	25.51	1,5-Anhydro-β-D-xylofuranose	57, 73, 86 (132)	H					0.97		0.57	1.13
67	25.89	2-Methyl-1H-indole	130, 129, 77	P		0.77	0.44	0.52				
68	26.13	Hydroquinone	110, 81, 55	L					2.76	0.77	1.61	2.62
69	26.87	Heptadecene	43, 57, 240	E	0.86	0.58	0.70	0.73				
70	27.17	Anhydrosugar	45, 57, 73	CH					1.35			1.22
71	27.40	Glycine-glycine DKP[c]	114, 86, 71	P	1.66		0.92	1.19	2.48	2.57	1.60	3.80
72	27.48	Acetoguaiacone	151, 166	L					0.74	0.57	0.61	1.98
73	27.59	2,3-Dimethyl-1H-indole	144, 145, 130	P	0.72	1.25	0.93	0.35				
74	27.76	3-Ethylguaiacol	152, 137	L	1.57	1.83	1.40	1.54	1.72	1.86	1.26	
75	28.30	4-Vinylsyringol	180, 165	L					0.68	0.54	0.37	1.39
76	28.47	Conyferyl alcohol	137, 180	L					0.86	0.57	0.50	1.40
77	29.50	Morpholin derivative	100	P	1.88	0.75	1.24	1.69	2.93	2.62	3.95	3.65
78	30.06	Anhydrosugar	73, 69, 85 (162)	CH					2.10			
79	30.28	1,6-Anhydro-β-D-glucopyranose (levoglucosan)	60, 57, 73 (162)	C	5.85	1.97	4.94	7.07	9.32	3.76	6.37	6.66
80	30.69	4-Propenylsyringol	194, 179	L					0.77	1.21	0.62	1.60
81	30.78	Pyrocoll	186, 93, 130	P	0.85	1.30	1.04	0.78	0.91	1.79	2.01	1.69
82	31.30	Morpholin derivative	100	P	3.86	1.38	3.19	3.86	5.00	5.47	6.74	6.24
83	32.36	Isoeugenol	164, 149	L					1.70	2.05	1.52	
84	32.40	Acetosyringone	181, 196	L					0.68	0.85	0.58	3.89
85	32.98	Hexadecanitrile	97, 110 (237)	E, P	1.23	7.67	5.54	0.92		2.75	1.38	
86	33.41	Proline-alanine DKP[c]	70, 168, 125, 97	P	1.63	0.70	1.39	2.02	2.20	2.00	2.41	1.86
87	34.17	n-Hexadecanoic acid	73, 129, 256	E	1.96			2.87	1.54	1.60	1.48	1.14
88	34.27	Proline-alanine DKP[c]	70, 168, 125, 97	P	2.10	0.92	1.30	2.48	1.63	1.59	1.73	1.86
89	34.57	Proline-valine DKP[c]	70, 72, 125 (196)	P	1.42	0.60	1.16	1.49	2.12	1.55	1.85	1.82
90	34.86	Proline-glycine DKP[c]	83, 70, 98 111, 154	P	2.55	2.99	4.37	3.90	2.20	2.42	2.34	2.32
91	35.17	2-(2-Hydroxyethyl)-piperidine	84, 41, 56 (129)	P	2.02	2.47	3.65	2.17				
92	35.31	Tiophene compound	114, 113, 85	P	1.61	1.73	2.04	1.46	1.11	1.28	0.74	1.85
93	35.48	Proline-arginine DKP[c]	154, 70, 125 (235)	P	1.58		1.61	2.41	1.55	2.16	2.60	2.58
94	35.98	Proline-isoleucine DKP[c]	154, 70, 125 (210)	P	1.31	2.12	2.62	1.60	1.94	2.13	2.64	1.94
95	36.09	Octadecanitrile	57, 97, 110 (265)	E, P		2.17	1.78			3.22	2.01	0.56
96	36.40	Proline-isoleucine DKP[c]	154, 86, 70, 125 (210)	P	1.98	0.80	1.87	2.59	2.04	2.66	2.85	1.97
97	36.43	Proline-proline DKP[c]	70, 194, 96, 138	P	1.84	1.04	1.76	1.84	1.42	1.69	2.02	2.03
98	36.93	Proline-leucine DKP[c]	70, 86, 154 (210)	P	1.75	1.67	2.21	1.86	2.23	2.54	3.26	3.30
99	37.02	Proline-leucine DKP[c]	70, 86, 154 (210)	P	1.62	1.36	2.32	1.73	2.77	2.86	3.42	4.35
100	37.51	1-Methyl-9H-pyrido(3,4-b)-indole (harmane)	182, 181, 154	E	0.85	1.76	2.10	1.21				
101	37.89	9H-Pyrido(3,4-b)-indole (β-carboline)	168, 140, 114	E	1.99	3.15	3.82	2.15	1.45	1.65	1.53	1.59
102	38.37	Hexadecanamide	59, 72, 128 (255)	E, P	2.44	1.20	2.95	3.14	1.46	1.69	1.83	1.76

a Possible origin of the identified compounds: C, cellulose; H, hemicellulose; L, lignin; CH, carbohydrate; E, extractive; P, protein.
b Total ion current (TIC) area % of the GC/MS peaks.
c DKP, 2,5-diketopiperazine.

Table 3. Relative Intensities (Summed TIC Area % Values) of the Major Groups of the Pyrolysis Products of Algae and Jatropha Samples with and without the Catalysts

Compounds' groups	Area % DAC	Area % DAC Fe/FSM-16	Area % DAC Fe/SBA-15	Area % DAC Fe_3O_4	Area % JSDC	Area % JSDC Fe/FSM-16	Area % JSDC Fe/SBA-15	Area % JSDC Fe_3O_4
Alkane, alkene	10.5	13.8	10.5	9.4	4.2	6.4	5.6	2.3
N-containing aromatics	12.7	16.0	12.5	12.0	7.7	6.9	7.8	6.9
Phenol-based aromatics	8.9	4.1	4.0	7.2	10.2	7.0	6.6	9.7
Aromatics with methoxy groups	1.6	1.7	1.4	1.5	11.2	9.4	9.5	15.6
Aromatic hydrocarbons	10.3	13.5	7.9	8.4	5.7	9.6	5.6	3.8
Anhydrosugars	6.6	2.0	4.9	7.7	14.9	3.8	7.3	10.3
Nitriles	4.6	17.1	11.7	5.8	1.9	9.2	4.8	1.8
2,5-Diketopiperazines[a]	20.2	13.5	22.6	23.9	23.5	25.8	28.6	29.5
Others	24.6	18.3	24.5	24.1	20.7	21.9	24.2	20.1

a Including pyrocoll (peak #81)

Comparing the overall pyrograms of DAC and JSDC, the composition of their pyrolysis oil seems to be similar. The main difference between them is the amount of the anhydrosugars and the aromatic lignin decomposition products. The DAC and JSDC samples contain 7.3 % and 24.2% of acid insoluble lignin, respectively (Table 1). Significantly more lignin monomeric compounds (peaks #**38**, **40**, **41**, **44**, **45**, **48-50**, **57**, **58**, **61**, **63**, **68**, **72**, **74-76**, **83** and **84**) were identified in the chromatograms of JSDC samples (Figure 4), which can be explained by the higher lignin content of this sample. Syringol monomers were not detected, only guaiacol and phenolic products were found in the pyrograms of the de-oiled algae cake, while de-oiled jatropha seed cake releases all the three types of lignin monomers. It is in agreement with the theory of lignin biosynthesis concluding that syringol lignin only exists in angiosperms.[43] The aromatic pyrolysis products originating from lignin and protein were categorized into the following groups: phenolics (without methoxy groups), methoxy-containing aromatics, and aromatic hydrocarbons. As Table 3 and Figure S2 show, the methoxy-containing aromatic

compounds (guaiacol and syringol derivatives) were released in similar yield with and without the catalysts. However, the yields of the phenolic compounds were significantly reduced in the presence of both silica supported iron catalysts. The formation of aromatic hydrocarbons was promoted by Fe/FSM-16 catalyst. The decrease of phenolic compounds is very important from the point of view of the possible utilization of the pyrolysis oil because phenols have acidic character and they are prone to polymerization, hence they reduce the stability of the pyrolysis oil.

The main decomposition product of cellulose pyrolysis is levoglucosan (peak #**79**). Other smaller anhydrosugar molecules (peaks #**47**, **55**, **66** and **78**) are also formed during the pyrolysis of cellulose and hemicellulose under inert atmosphere. The intensities of the carbohydrate decomposition products are higher during the pyrolysis of JSDC than that of DAC sample in agreement with the considerably higher cellulose and hemicellulose content of the raw material (see Table 1). The yields of levoglucosan and other anhydrosugar molecules reduced significantly in the presence of silica supported iron catalysts (Fe/FSM-16 and Fe/SBA-15) (Table 3 and Figure S2). The glucopyranose and glucofuranose derivatives probably decomposed into more stable smaller molecules (e.g., acetone) on the surface of the catalysts. Fe/FSM-16 is much more effective catalyst for carbohydrates than Fe/SBA-15. The presence of Fe_3O_4 did not modify the decomposition routes of carbohydrates notably.

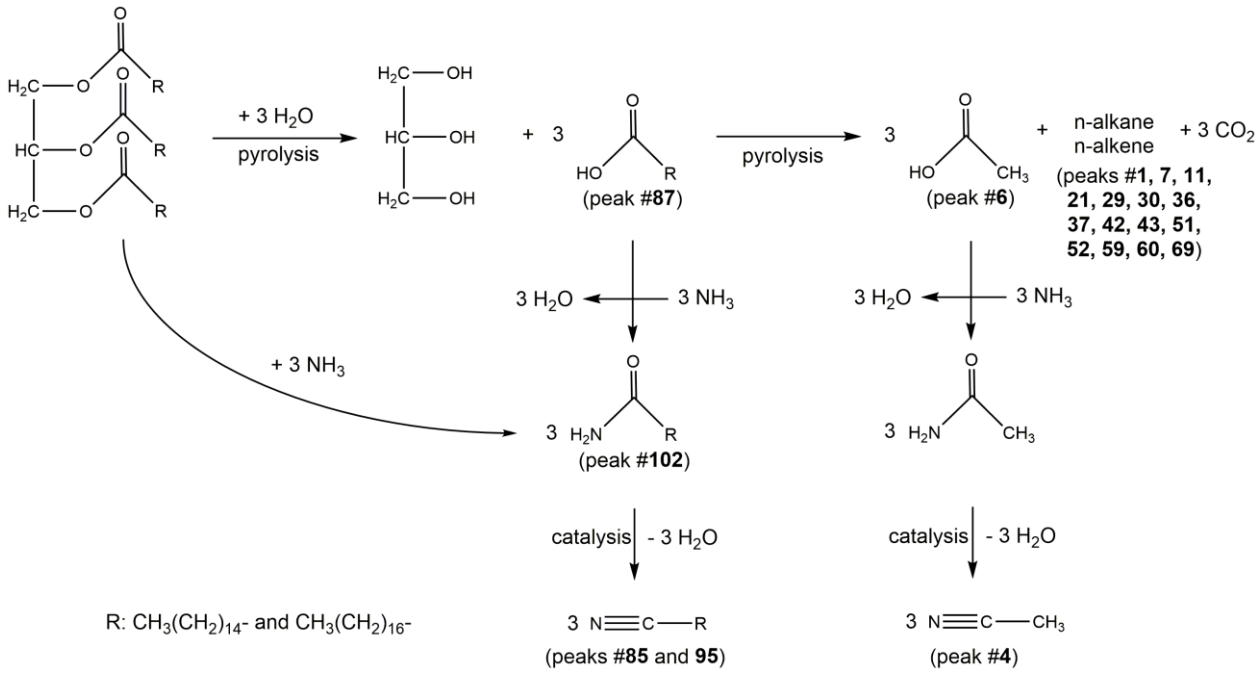

Figure 5. Possible pathways of the nitrile formation from triglycerides using catalysts.

The de-oiled biomass samples still contain small amounts of triglycerides, which decompose into fatty acids and glycerin during the pyrolysis as illustrated in Figure 5. These fatty acids are mostly palmitic acid (peak #**87**) and probably stearic acid. Alkanes (peaks #**29**, **36**, **42, 51** and **59**), alkenes (peaks #**1**, **7**, **11**, **21**, **30**, **37**, **43**, **52**, **60** and **69**), carbon dioxide (Figure 2 and S1) and acetic acid (peak #**6**) can be formed by further decomposition reaction of the fatty acid molecules as presented in Figure 5. In the presence of Fe/FSM-16 and Fe/SBA-15 catalysts, nitrile molecules (acetonitrile, peak #**4**), hexadecanitrile (peak #**85**) and octadecanitrile (peak #**95**) were released during the reaction of fatty acids and ammonia originated from protein (Table 2). Without catalysts or in the presence of Fe_3O_4, smaller amounts of acetonitrile, hexadecanitrile and at most only traces of octadecanitrile were measured in the pyrolysate (Figure 3a, 3d, 4a, 4d and Table 2). The formation of nitrile molecules was the most pronounced when Fe/FSM-16

catalyst was used. Hexadecane amide (peak #**102**), a possible intermediate of the formation of hexadecanenitrile was also identified among the decomposition products.

The main nitrogen-containing decomposition products at higher retention times are 2,5-diketopiperazines (DKPs) (peaks #**86**, **88**-**90**, **93**, **94** and **96**-**99**). These molecules are the thermal decomposition products of proteins.[41] The protein content of DAC and JSDC are 20.5% and 28.8%, respectively (Table 1). Adamiano et al. established that small amounts of iron on chrysotile nanofiber decreased the DKP formation from bovine serum albumin during off-line pyrolysis.[44] A similar reduction was observed in the relative intensities of DKPs during the pyrolysis of DAC using Fe/FSM-16 catalyst. However, this change was not observed under other experimental conditions, as it can be seen in Table 3 and Figure S2. Further experiments are needed to clarify, which conditions influence the DKP yield during the catalytic pyrolysis of protein-containing biomass.

Indole (peak #**62**) and its derivatives as 3-methyl-1H-indole (peak #**65**) are likely to be formed by the fragmentation of the amino acid, tryptophan and alkaloids. Two plant alkaloids were identified in the pyrolyzate: β-carboline (peak #**101**) (9H-pyrido-(3,4-b)-indole) and the blood harmane (peak #**100**) (1-methyl-9H-pyrido-(3,4-b)-indole), which may produce smaller indole derivatives. Pyrrole (peak #**13**) and its derivatives (peaks #**20**, **22**, **24**, **26** and **27**) are the building blocks of biologically important nitrogen-containing compounds, like chlorophylls, vitamins, vegetable hormones and amino acids (proline and hydroxyproline). The concentration of pyrrole compounds increased significantly in the pyrolyzate using Fe/FSM-16 catalyst, while it did not change significantly in the presence of the Fe/SBA-15 catalyst during the pyrolysis of both DAC and JSDC samples. Although the applied catalysts had some effects on the yield of nitrogen-

containing products, they are not suitable for reducing the nitrogen-content of the pyrolysis oil significantly.

4 CONCLUSION

The thermal decomposition of two different by-products of biodiesel production process (de-oiled algae cake and jatropha seed de-oiled cake) was studied by TG/MS and Py-GC/MS in order to test their suitability for bioenergy generation. The composition of the organic constituents (carbohydrate, lignin, and protein content) was determined by acidic hydrolysis followed by HPLC analysis and the Dumas method. The inorganic ion content was characterized by ICP-OES. The effect of two silica supported iron catalysts (Fe/FSM-16 and Fe/SBA-15) and magnetite (Fe_3O_4) was tested on the yield of the decomposition products.

Magnetite had no systematic effect on the pyrolysis product distribution of the by-products; however, mesoporous silica supported iron catalysts affected the yield of several compounds considerably. Decreased decomposition rate was observed in the temperature range of the main organic components (200-400 °C) in the presence of silica based catalysts, while increased yield of hydrocarbons was measured between 400 and 550 °C originating from the residual oil content of the samples. Hydrogen and carbon monoxide evolution significantly increased during the carbonization process at higher temperatures (550-900 °C).

Substantial part of the anhydrosugar molecules was cracked by the silica based iron catalysts indicated by their reduced yield and enhanced formation of some ketones (e.g., acetone). The evolution of acetic acid and phenolic compounds was hindered by the supported catalysts, which points to the reduced acidity of the pyrolysis oil. Another advantage of the lower yield of the phenolics is that the susceptibility of the oil to polymerization must be decreased. The reduced

acidity and the increased stability of the pyrolysis oil are among the main objectives of the catalytic pyrolysis of biomass samples.

The main decomposition products of proteins under inert atmosphere are 2,5-diketopiperazines, their yields were not influenced systematically by the studied catalysts. One of the major effects of the silica based catalysts is the promotion of nitrile formation. In the presence of Fe/FSM-16 or Fe/SBA-15 catalysts, the reaction between fatty acid molecules originating from triglycerides and ammonia derived from amino acids were promoted, and long chain nitriles appeared in the pyrograms.

Acknowledgement

This work is dedicated to the memory of Prof. Michael J. Antal Jr. This work was supported by NKFIH, Hungary & DST, India through the Bilateral Cooperation between Hungary (project No. TÉT_13_DST-1-2014-0003) and DST-India (DST/INT/HUN/P-02/2014) and "Bolyai János" research fellowship.

Supporting Information

Figure S1 shows the TG/MS curves of Jatropha seeds de-oiled cake with and without the catalysts. Figure S2 illustrates the relative intensities of the major groups of the pyrolysis products of DAC and JSDC samples with and without the catalysts.

References

(1) Bi, Z.; He, B.; McDonald, A. G. *Energy Fuels* **2015**, *29*, 5018-5027.

(2) Wahlen, B. D., Morgan, M. R., Mc Curdy, A. T.; Willis, R. M.; Morgan, M. D., Dye, D. J.; Bugbee, B.; Wood, B. D.; Seefeldt, L. C. *Energy Fuels* **2013**, *27*, 220-228.

(3) Oncel, S. S. *Renew. Sustain. Energy Rev.* **2013**, *26*, 241-264.

(4) Zhu, Y.; Piotrowska, P.; van Eyk, P. J.; Boström, D.; Kwong, C. W.; Wang, D.; Cole, A. J.; de Nys, R.; Gentili, F. G.; Ashman, P. J. *Energy Fuels* **2015**, *29*, 1686-1700.

(5) Spolaore, P.; Joannis-Cassan, C.; Duran, E.; Isambert, A. *J. Biosci. Bioeng.* **2006**, *101* (2), 87-96.

(6) Krohn, B. J.; McNeff, C. V.; Yan, B.; Nowlan, D. *Bioresour. Technol.* **2011**, *102*, 94-100.

(7) Patil, P. D.; Gude, V. G.; Mannarswamy, A.; Deng, S.; Cooke, P.; Munson-McGee, S.; Rhodes, I.; Lammers, P.; Nirmalakhandan, N. *Bioresour. Technol.* **2011**, *102*, 118-122.

(8) Sathish, A.; Sims, R. C. *Bioresour. Technol.* **2012**, *118*, 643-647.

(9) Melis, A.; Happe, T. *Plant Physiol.* **2001**, *127*, 740-748.

(10) Neef, H. J. *Energy* **2009**, *34*, 327-333.

(11) Fayaz, H.; Saidur, R.; Razali, N.; Anuar, F. S.; Saleman, A. R.; Islam, M. R. *Renew. Sustain. Energy Rev.* **2012**, *16*, 5511-5528.

(12) Ververis, C.; Georghiou, K.; Danielidis, D.; Hatzinikolaou, D. G.; Santas, P.; Santas, R.; Corleti, V. *Biores. Technol.* **2007**, *98*, 296-301.

(13) Kaushik, N.; Kumar, K.; Kumar, S.; Kaushik, N.; Roy, S. *Biomass Bioenergy* **2007**, *31* (7), 497-502.

(14) Ajayebi, A.; Gnansounou, E.; Raman, J. K.; *Biores. Technol.* **2013**, *150* 429-437.

(15) Eshton, B.; Katima, J. H. Y.; Kituyi, E. *Biomass Bioenergy* **2013**, *58*, 95-103.

(16) Mofijur, M.; Masjuki, H. H.; Kalam, M. A.; Hazrat, M. A.; Liaquat, A. M.; Shahabuddin, M.; Varman, M. *Renew. Sustain. Energy Rev.* **2012**, *16*, 5007-5020.

(17) Sabandar, C. W.; Ahmat, N.; Jaafar, F. M.; Sahidin, I. *Phytochem.* **2013**, *85*, 7-29.

(18) Devappa, R. K.; Roach, J. S.; Makkar, H. P. S.; Becker, K. *Ecotox. Environ. Saf.* **2013***, 94*, 172-178.

(19) Li, C. Y.; Devappa, R.K.; Liu, J. X.; Lu, J. M.; Makkar, H.P.S.; Becker, K. *Food Chem. Toxic.* **2010**, *48*, 620-625.

(20) Wang, K. G.; Brown, R.C. *Green Chem.* **2013**, *15* (3), 675-681.

(21) Zhao, D.; Feng, J.; Hou, Q.; Melosh, N.; Fredrickson, G. H.; Chmelka, B. F.; Stucky, G.D. *Science* **1998**, *279*, 548-552.

(22) Zhao, D.; Yang, P.; Melosh, N.; Feng, J.; Chmelka, B. F.; Stucky, G.D. *Adv. Mater.***1998**, *10* (16), 1380-1385.

(23) Yan, H.; Chen, W.; Liao G.; Li, X.; Ma, S.; Li, L. *Sep. Purif. Technol.* **2016**, *159*, 1-6.

(24) Palacio, R.; Gallego, J.; Gabelica, Z.; Batiot-Dupeyrat, C.; Barrault, J.; Valange, S. *Appl. Catal. A: Gen.* **2015**, *504*, 642-653.

(25) Yanagisawa, T.; Shimizu, T.; Kuroda, K.; Kato, C. *Bull. Chem. Soc. Jpn.* **1990**, *63*, 988-992.

(26) O'Brien, S.; Francis, R. J.; Fogg, A.; O'Hare, D.; Okazaki, N.; Kuroda, K. *Chem. Mater.* **1999**, *11*, 1822-1832.

(27) Tuzoka, Y.; Wongmekiat, A.; Kumira, K.; Moribe, K.; Yamamura, S.; Yamamoto, K. *Chem. Pharm. Bull.* **2005**, *53* (8), 974-977.

(28) Sakata, Y.; Uddin, M. A.; Muto, A. *J. Anal. Appl. Pyrol.* **1999**, *51*, 135-155.

(29) Bachari, K. Guerroudj, R. M.; Lamouchi, M. *Kinet. Catal.* **2011**, *52* (1), 119-127.

(30) Boudjemaa, A.; Bachari, K.; Trari, M. *Mater. Sci. Semicond. Process.* **2013**, *16*, 838-844.

(31) Bhaskar, T.; Uddin, M. A.; Muto, A.; Sakata, Y.; Omura, Y.; Kimura, K.; Kawakami, Y. *Fuel* **2004**, *83*, 9-15.

(32) Munoz, M.; de Pedro, Z. M.; Casas, J. A.; Rodriguez, J. J. *Appl. Catal. B: Environmental*, **2015**, *176–177*, 249-265.

(33) Mostafa, A.; El-Dissouky, A.; Fawzy, A.; Farghaly, A.; Peu, P.; Dabert, P.; Le Roux, S.; Tawfik, A. *Biores. Technol.* **2016**, *216*, 520-528.

(34) Watson, M. E.; Galliher, T. L. *Commun. Soil Sci. Plant Anal.* **2001**, *32*, 2007-2019.

(35) Sluiter, A.; Hames, B.; Ruiz, R.; Scarlata, C.; Sluiter, J.; Templeton, D.; Crocker, D. **2008**, National Renewable Energy Laboratory

(36) Sebestyén, Z.; May, Z.; Réczey, K.; Jakab, E. *J. Therm. Anal.Calorim*. **2011**, *105*, 1061-1069.

(37) Csikkel-Szolnoki, A.; Báthori, M.; Blunden, G. *Microchem. J.* **2000**, *67*, 39-42.

(38) Sebestyén, Z.; Jakab, E.; May, Z.; Sipos, B.; Réczey, K. *J. Anal. Appl. Pyrol.* **2013**, *101*, 61-71.

(39) Faix, O.; Meier, D.; Fortmann, I. *Holz Roh Werkst.* **1990**, *48*, 351-354.

(40) Faix, O.; Fortmann, I.; Bremer, J.; Meier, D. *Holz Roh Werkst.* **1991**, *49*, 299-304.

(41) Fabbri, D.; Adamiano, A.; Falini, G.; De Marco, R.; Mancini, I. *J. Anal. Appl. Pyrol.* **2012**, *95*, 145-155.

(42) Kurata, S.; Ichikawa, K. *Bunseki Kagaku* **2008**, *57* (7), 563-569.

(43) Novo-Uzal, E.; Pomar, F.; Ros, L.V.G.; Espineira, J.M.; Barcelo, A.R. *Adv. Bot. Res.* **2012**, *61*, 311-350.

(44) Adamiano A.; Lesci I.G.; Fabbri, D.; Roveri, N. *J. R. Soc. Interface* **2015**, *12* (107), 20150186

Supporting information

Thermoanalytical characterization and catalytic conversion of de-oiled micro algae and jatropha seed cake

Zoltán Sebestyén[1], Eszter Barta-Rajnai[1], Zsuzsanna Czégény[1], Thallada Bhaskar[2], Bhavya B. Krishna[2], Zoltán May[1], János Bozi[1], Zsolt Barta[3], Rawel Singh[2], Emma Jakab[1]

[1]*Institute of Materials and Environmental Chemistry, Research Centre for Natural Sciences, Hungarian Academy of Sciences, Magyar Tudósok körútja 2, H-1117 Budapest, Hungary*

[2] *Bio-Fuel Division (BFD), CSIR-Indian Institute of Petroleum (IIP), Mohkampur, Dehradun-248005, Uttarakhand, India*

[3]*Department of Applied Biotechnology and Food Science, Budapest University of Technology and Economics, H-1111 Budapest, Szent Gellért tér 4, Hungary*

S3 RESULTS AND DISCUSSION

S3.2 TG/MS results. Figure S1 shows the TG/MS curves of jatropha seed de-oiled cake (JSDC) with and without catalysts. Two main differences can be observed in the decomposition pattern between JSDC (Figure S1a) and de-oiled algal cake (DAC, Figure 2a in the main paper). The DTG curve has a pronounced shoulder and several MS intensity curves of JSDC have peaks at about 280 °C, which can be attributed to the thermal decomposition of hemicellulose. The hemicellulose content of JSDC is about 5 times higher than that of DAC (Table 1); hence the hemicellulose peaks can be clearly distinguished. The other difference between the two samples is due to the different amounts of inorganic materials. DAC has a high calcium carbonate content, which decomposes at about 700 °C releasing high yield of CO_2. This decomposition step is missing during the decomposition of JSDC. Thus the carbon dioxide evolution can be better seen

at lower temperatures. The first CO_2 peak appears at 200-320 °C, which can be derived from hemicellulose. The second CO_2 peak at about 350 °C can be attributed to the cellulose decomposition.

The effect of silica supported iron catalysts and Fe_3O_4 is very similar on the JSDC sample than on DAC discussed in the main part of the paper. Decreased yield of ammonia (*m/z* 17) can be observed using the catalysts. The silica supported iron catalysts promote the release of aliphatic compounds from the residual oil content of the samples, which is indicated by the increased intensity of ethyl groups (*m/z* 29) between 400 and 600 °C (Figure S1b and c). The char formation is enhanced by the silica supported iron catalysts, which is reflected by the evolution curves of hydrogen and carbon monoxide. The char oxidation occurs in the presence of magnetite (Figure S1d) above 600 °C similarly to DAC, which is indicated by the formation of carbon dioxide.

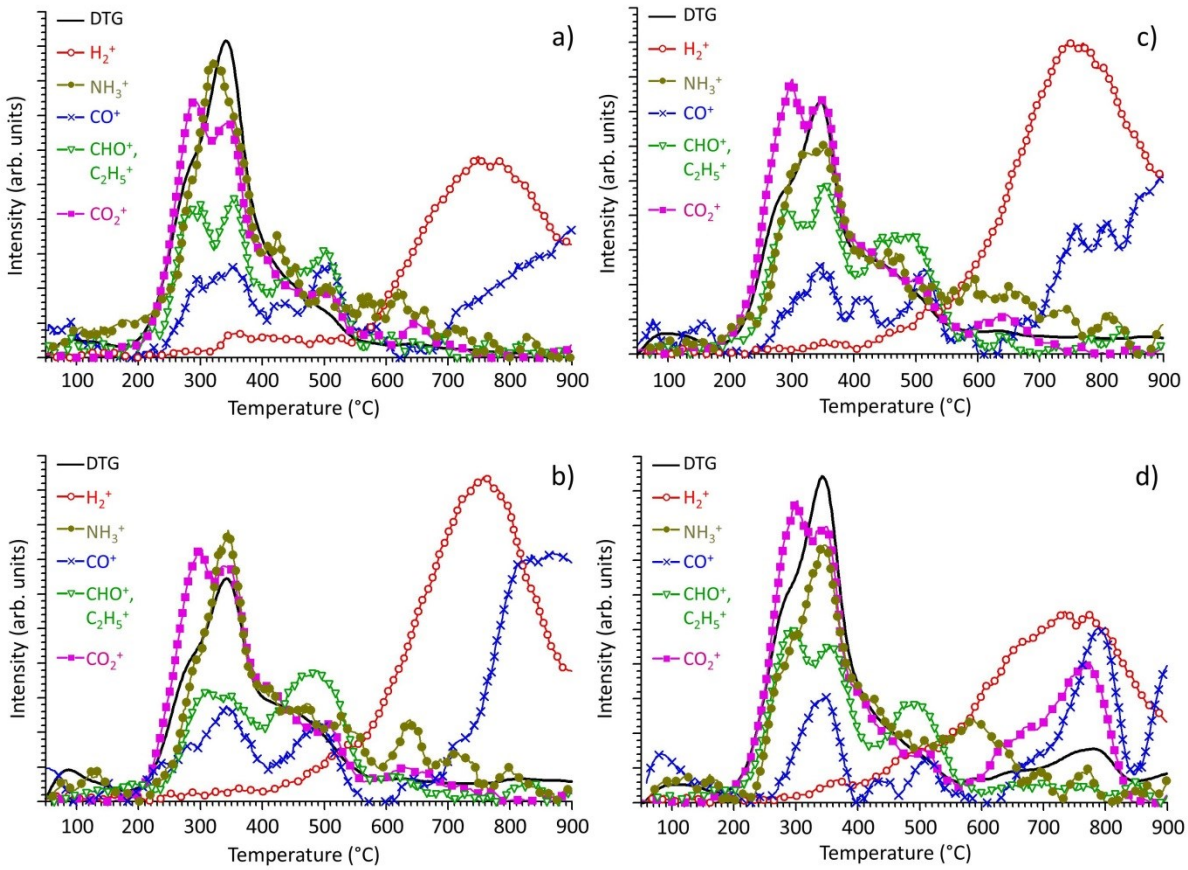

Figure S1. Evolution profile of the main gaseous decomposition products (*m/z* 2, hydrogen;*m/z* 17, ammonia; *m/z* 28, carbon monoxide; *m/z* 29, formyl and ethyl groups; *m/z* 44, carbon dioxide) derived from the jatropha seed de-oiled cake (JSDC) (a) without catalysts, in the presence of (b) Fe/FSM-16, (c) Fe/SBA-15, and (d) Fe_3O_4 catalysts.

S3.3 Pyrolysis results. Figure S2 presents the pie charts of the pyrolysis yields of the main compound groups in case of DAC and JSDC with and without the catalysts. The effect of the catalysts is discussed in the main paper, where these data are found in Table 3.

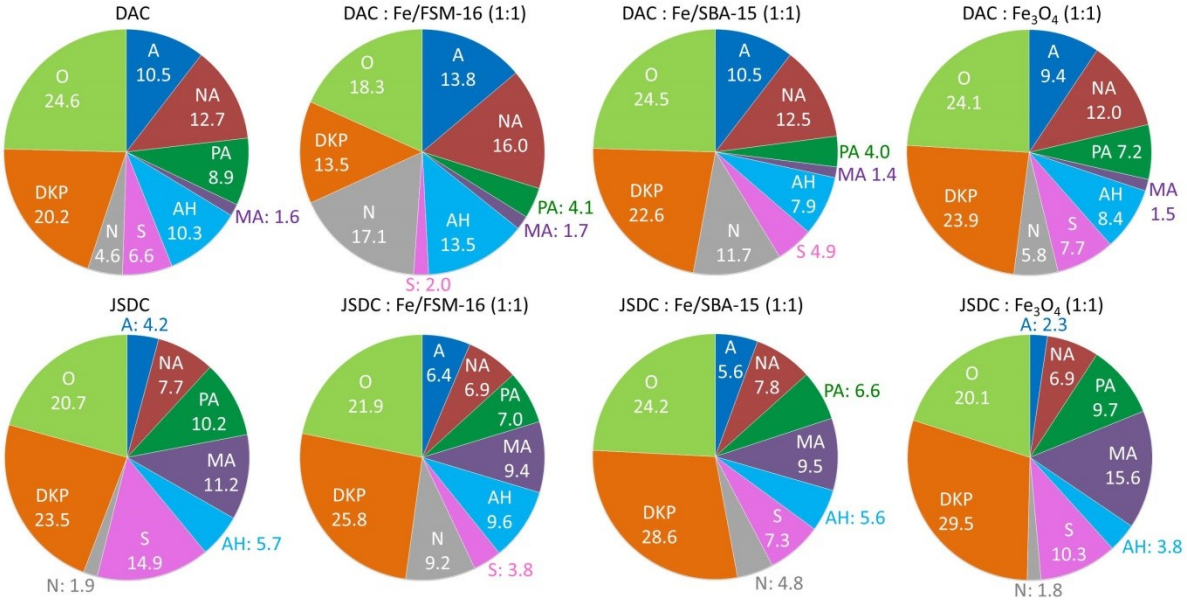

Figure S2. Pie Charts of the Relative Intensities (Summed TIC Area % Values) of the Major Groups of the Pyrolysis Products of Algae and Jatropha Samples with and without the Catalysts; The Groups Represented by the Letters are: A, Alkane, Alkene; NA, Nitrogen-containing Aromatics; PA, Phenol-based Aromatics; MA, Methoxy group-containing Aromatics; AH, Aromatic Hydrocarbons; S, Anhydrosugars; N, Nitriles; DKP, 2,5-Diketopiperazines (Including Pyrocoll Peak #81) and O, Others.